High Resolution ATR μ-FTIR to map the diffusion of conservation treatments applied to painted plasters

Noemi Calore [a], Alessandra Botteon[b], Chiara Colombo[b], Alessandro Comunian[a], Elena Possenti[a,b], Marco Realini[b], Diego Sali[c], Claudia Conti[b]*

[a] *Dipartimento di Scienze della Terra, Università degli Studi di Milano, Via Mangiagalli 34, 20133, Milano, Italy*

[b] *Consiglio Nazionale delle Ricerche, Istituto per la Conservazione e la Valorizzazione dei Beni Culturali (ICVBC), Via Cozzi 53, 20125, Milano, Italy*

[c] *Bruker Italia S.r.l. Unipersonale, V. le V. Lancetti 43, 20158, Milano, Italy*

* Corresponding author's email address: c.conti@icvbc.cnr.it

Abstract

Here we demonstrate the extension of applicability of high resolution Attenuated Total Reflection Fourier transform infrared μ-mapping (ATR μ-FTIR) to the investigation of the diffusion of ammonium oxalate, an inorganic mineral conservation treatment, within painted plasters. The method demonstrates its potentiality in situations where high lateral resolution is required and the compounds are not easily detectable with conventional analytical techniques. It was applied successfully to explore the interaction between ammonium oxalate solutions and the carbonatic matrix at the microscale. The reaction of the carbonatic aggregate particles was assessed as well as the influence of the treatment parameters on the penetration depth. High resolution ATR μ-FTIR represents a new spectroscopy imaging modality expanding the portfolio of chemically specific analytical tools.

Introduction

Inorganic mineral products are increasingly used in restoration works of artistic surfaces due to their compatibility and durability with inorganic matrixes. They produce insoluble phases either by solution precipitation of compounds or chemical reaction with the carbonatic substrate [1]. The

crystallization of a product with high affinity with the inorganic substrate and more resistant to the decay is successful in reconstructing the degraded matrices. However, the evaluation of the diffusion of treatments within the material microstructure and their penetration depth is challenging, and at the same time plays a key role in a conscious assessment of their actual efficacy [2-4]. The conventional analytical methods used so far for achieving information on treatment distribution underneath the treated surface have proven not to give satisfactory results. The main acknowledged challenges include the limited lateral resolution and the inability to fully discriminate between the newly formed phases and the matrix due to a similar chemical composition. Advanced methods have been also recently experimented as neutron-based techniques [5,6]; hydrogen, marker element of the newly phases formed after the treatment, has a high neutron scattering and the detection of its distribution can be used to obtain a non-destructive 3D representation of the treated and not treated portions of the material. However, the available data in literature have been acquired with a spatial resolution around 100 μm, which is excellent for achieving a diffusion overview but it is not suitable to gain a refined knowledge of the micrometric network; moreover, it is a not easily accessible tool to be used in daily experiments.

Micro-spectroscopy is one of the most promising field in this context, permitting a good discrimination power and a high lateral resolution with conventional laboratory instruments [7-12]. For this reason, μ-Raman mapping has been used to study the diffusion of ammonium oxalate [$(NH_4)_2(C_2O_4)$] treatment applied to model samples of painted plasters [13,14]. Ammonium oxalate aqueous solution reacts with the substrate changing the carbonate phases into calcium oxalate crystalline phases, thus reconstructing the decayed portions of the matrix [15,16]. Penetration depth, diffusion and interaction between product and the matrix components have been successfully assessed; however, especially dealing with real case studies, μ-Raman spectroscopy suffers of important limitations such as fluorescence and thermal effects which can completely overwhelm any possible Raman signal.

μAttenuated Total Reflection Fourier Transform Infrared Spectroscopy (ATR μ-FTIR) has been already tested for investigating the penetration depth of organic polymeric treatments, demonstrating its ability on obtaining depth profiles of the product with a lateral resolution ranging from 50 μm to 100 μm [2]. A synchrotron-based μ-FTIR instrument was used to map the surface distribution of ammonium oxalate treated samples, reaching a lateral resolution down to 5 μm [17]; despite the instrument cannot be used in routine experiments, this study demonstrated the strong potentiality of a method which combines the inherently high chemical specificity of FTIR with a high lateral resolution.

Here we suggest the application of high resolution ATR μ-FTIR technique, recently developed, as an ideal laboratory method for the investigation of the diffusion of ammonium oxalate treatment within painted plasters at the microscale. A recent study [18] demonstrated the potential of this technique dealing with the identification of the chemical composition of thin layers coming from painted stratigraphy of prestigious artworks, with a lateral resolution down to 5 μm, high spectral quality and chemical image contrast. A parallel protocol is here proposed, with the aim to overcome the limitations of the current analytical methods and to offer to the conservation science community an innovative and effective alternative for the investigation of the inorganic and organic treatments diffusion .

Materials

The model samples consist of a plaster layer (3 mm thick) made by a lime binder and calcareous powder aggregate (ranging from 1 μm to 500 μm). The binder/aggregate ratio is 1:3. A yellow ochre pigment (goethite) was applied by *a fresco* technique on the plaster layer. The substrate is an Italian calcareous stone.

The carbonation of the specimens was obtained by a 4 months permanence in a wet box with a carbon dioxide enriched atmosphere to induce the complete transformation of portlandite $Ca(OH)_2$ into calcite ($CaCO_3$).

After the complete carbonation of the plasters, a 5 % w/v solution of ammonium oxalate was applied by a cellulose poultice on the sample surface. The poultice of cellulose pulp contains a dispersion of approximately 18 ml of ammonium oxalate solution and the poultice/solution ratio is 5 . Three different treatment conditions were selected:

- 5 hours of contact time, with the addition of 4.8 ml of ammonium oxalate solution (ca. 1.2 ml/hour): Sample A
- 5 hours of contact time, with no solution addition: Sample B
- 8 hours of contact time, with no solution addition: Sample C

Thin cross sections of the samples were prepared for the observation in polarized optical microscopy and analysis with high resolution ATR μ-FTIR. The same areas observed by polarized optical microscopy were analysed with high resolution ATR μ-FTIR in order to correlate mineralogical observations with molecular composition.

Methods

Polarized optical microscopy

Microscopic observations have been carried out by a polarizing microscope (Nikon Eclipse E400 Pol.), equipped with a digital image capturing system. For each thin cross section, the most meaningful areas were identified and images at different magnifications (2×, 4×, 10×, 20×, and 40×) were acquired in order to identify the same areas with FTIR microscope. The area have been selected with the aim to cover all the observed situations, i.e. areas with preponderance of *a fresco* painted layer, plaster binder or aggregate, presence of fractures.

High resolution µAttenuated Total Reflection Fourier Infrared Spectroscopy

ATR µ-FTIR analyses were carried out on thin cross sections with a LUMOS Standalone FTIR microscope (Bruker Optik GmbH), which includes an interferometer (RockSolidTm permanently aligned), an automated XYZ sample stage and a mid band 100 µm × 100 µm PC-MCT detector. The objective and the condenser have low magnification (8x) for the visible inspection of the sample and all the optics and the beamsplitter are in ZnSe to avoid problems related to higroscopicity. The standard spectral range goes from 7000 cm^{-1} to 650 cm^{-1} and the maximum spectral resolution is 0.8 cm^{-1}. The probe with ATR germanium frustum of cone-shaped crystal (tip diameter about 100µm) makes contact with the sample at selected pressure values (low, medium, high), and the motorized sample stage allows ATR mapping with an IR aperture down to 4 µm × 4 µm. Chemical images were acquired and manipulated with OPUS-IR™ software (Bruker Optik GmbH, version 7.5) and generated by band correlations; this modality compares the shape of one band of a detected compound with the shape of the same band of the pure compound spectrum. The concentration scale, then, is generated according to how much the band shape of the single spectrum of the map is similar to the band shape of the pure compound. This modality is more accurate than the conventional integration band and it has been considered more suitable to determine calcium oxalate distribution. The ratio between calcite and calcium oxalate was also evaluated by averaging the spectra acquired in a map; in this way, representative spectra of the mapped regions were achieved and compared.

Several maps were obtained with low pressure, 32 scans and 4 µm × 4 µm aperture, which corresponds to a 1 µm × 1 µm aperture dimension in the IR due to the germanium crystal magnification. Around 3.5 µm step size (along *x* and *y,* corresponding to 0.9 µm in the IR) was

chosen to create moderate oversampling during the mapping, increasing the SNR and image contrast.

To obtain straightforward information about the reaction of ammonium oxalate with the aggregate particles, in selected maps the higher and lower values of the colour scale were changed in order to stress the transition regions: the higher value was decreased down to reach the edge of the aggregates, the lower one was increased up to eliminate any false signal of calcium oxalate.

It is worth noting that the method is micro-destructive since the investigated area is slightly damaged by germanium crystal imprint [18]. For this reason, the optical images were acquired before ATR μ-FTIR analyses to ensure a confident comparison between the optical images and their relative maps.

Results and discussion

The polarized optical microscopy observations of the thin cross sections show an isotropic orientation of aggregate particles, including both crystals and sedimentary rock fragments, dispersed in the micritic carbonatic matrix of the plaster. Crystals consist of calcite or dolomite, whilst sedimentary rock fragments are mainly composed by calcite. The aggregate particles size is very poorly sorted; they present a variable degree of sphericity, from subrounded to angular. The plaster has a low porosity but, mainly in sample C, macro fractures within the plaster are clearly observed. In the uppermost part of the plaster tabular carbonatic aggregates shows a preferential horizontal orientation, due to the final process of the plaster application. In line with expectations the observation by polarized optical microscopy does not provide information about the presence of calcium oxalate crystals formed after ammonium oxalate treatment due to their extremely tiny size (down to 1 μm).

For each sample, the most significant areas were selected for the investigations by ATR μ-FTIR in order to shed light on the interaction of ammonium oxalate treatment with the *a fresco* painted layer, the plaster binder and the aggregates particles. Moreover, a sequence of areas located at different depths were chosen to investigate the penetration depth achieved by the treatment and the influence of the fractures on its diffusion.

The FTIR patterns of the main crystalline phases (*e.g.* calcite, dolomite, calcium oxalate) and organic compound (embedding resin) of the thin sections have been identified by ATR μ-FTIR and compared to those of references. In order to obtain the distribution map of each identified compound, its most characteristic absorption bands were selected for correlation (Figure 1). The attribution of the FTIR bands of the detected compounds is shown in Table 1. Carbonates, which

constitute the binder (calcite) as well as the aggregates (calcite and dolomite) of the plaster, are characterized by several characteristic bands due to CO_3^{2-} groups vibrations [19]. Among them, the band localized between 750 cm^{-1} and 700 cm^{-1} was used for the correlations, as it varies in frequency depending on the content of magnesium and therefore allows distinguishing different carbonate crystalline phases (calcite between 720 cm^{-1} and 705 cm^{-1} and dolomite between 740 cm^{-1} and 720 cm^{-1}). No differences were observed between calcite peaks of the aggregate and of the binder. Epoxy resin, used for the embedding, was detected outside the plaster and within the samples as well, filling the voids (porosity and fractures) of the binder. The band localised between 1255 cm^{-1} and 1240 cm^{-1} was considered to plot the distribution map, as this range is relatively free from overlapping with other vibrations. Calcium oxalates, in the crystalline form of whewellite ($CaC_2O_4 \cdot H_2O$) and weddellite [$(CaC_2O_4 \cdot (2 + x)H_2O)$], are formed after the ammonium oxalate treatment [5]. These two phases are characterized by extended overlapping of their vibrational bands in the same spectral regions, making the identification of individual crystalline phases quite complex in case of mixture of the two compounds. Therefore, in this study, whewellite and weddellite are both labelled "calcium oxalate" and they are mapped together correlating their characteristic strong band between 1325 cm^{-1} and 1305 cm^{-1} [20]. The band located between 915 cm^{-1} and 905 cm^{-1} allows the identification of goethite [21], the yellow pigment of the *a fresco* painted layer. No iron by-products were detected after the ammonium oxalate treatments, confirming that no reaction occurs between the reagent and the pigment. Newly-formed Mg compounds might form as well, due to the reaction of ammonium oxalate with dolomite aggregates. However, the presence of magnesium by-products as Mg-oxalates (*e.g* glushinskite, $Mg(C_2O_4)\cdot 2H_2O$), potentially well distinguishable from whewellite and weddellite, was not ascertained, also due to the severe bands overlapping; for instance, glunshinskite is characterized by the absorption between 840 cm^{-1} and 820 cm^{-1} [22], which is overlapped with the resin band. Nevertheless, the release of Mg^{2+} ions from dolomite is even more delayed than Ca^{2+} ions [23], thus the absence of Mg- oxalates is quite expected.

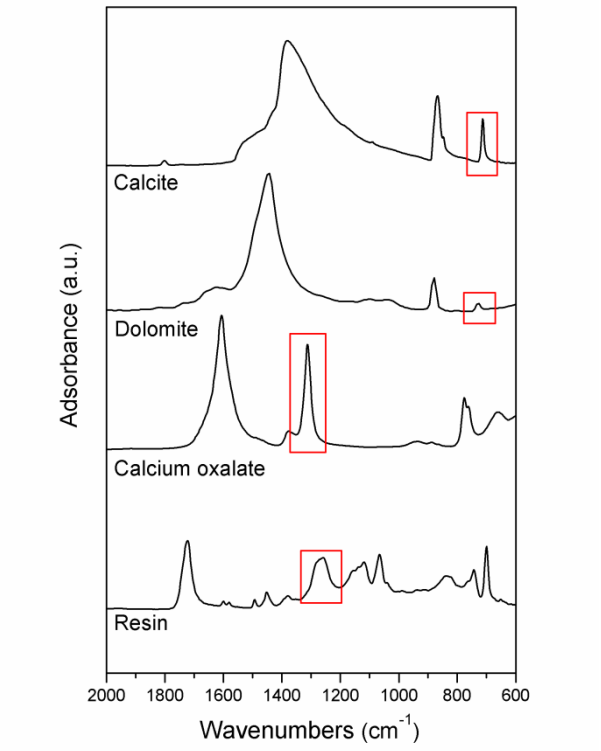

Figure 1: FTIR patterns of calcite, dolomite, calcium oxalate and embedding resin identified by ATR µ-FTIR in the samples.

Substance	**Detected IR bands**	**Assignment**	**References**
Calcite	1450-1380 s	ν_{as} CO_3^{2-}	[19]
	890-860 m	$\delta_{out\text{-}of\text{-}plane}$ CO_3^{2}	
	725-705 m *	$\delta_{in\text{-}plane}$ CO_3^{2}	
Dolomite	740-725 m *	$\delta_{in\text{-}plane}$ CO_3^{2}	[19]
Epoxy resin	2934 s, 2869 s	ν $-CH_2$, $-CH_3$	[24]
	1260-1210 s *, 1050-1010 m	ν_{as} $-O-CH_2-$	
	1195-1175 s, 1130-1108 m-w	$\delta_{out\text{-}of\text{-}plane}$ C-H	
	840-820 m	$\delta_{out\text{-}of\text{-}plane}$ $C\text{-}H_{aromatic\ ring}$	
Calcium oxalate	3600-3000 w br	ν OH	[20]
	1650-1580 s	ν C=O	
	1380-1360 w	ν C-C and C-O	
	1325-1305 s *		
	790-770 m	δ C-H	
	695-685 m	δ OH	
Goethite	915-905 m-w *	δ OH	[21]

Table 1 FTIR bands (cm^{-1}) and vibrational assignments of the substances detected in the thin cross sections. The marker * indicates the bands selected for correlations. The bands intensity is indicated with ''w'' weak, ''m'' medium, ''s'' strong, ''br'' broad.

High resolution ATR μ-FTIR mapping turned out to be very sensitive to investigate the calcium oxalate distribution.

In *a fresco* painted layer of each sample, calcite of the binder is surprisingly deeply substituted by newly-formed calcium oxalate (Figure 2). The high reactivity of the layer is most likely due to: (i) the very high specific area of micritic calcite, with a consequent relevant reaction rate with ammonium oxalate solution; (ii) its direct contact with the poultice during the treatment, which implies that it is the first portion of the specimen to react with ammonium oxalate (iii) the relative high amount of available reagent. The strong presence of calcium oxalate in *a fresco* painted layer is also confirmed by the average spectrum in which the band of calcium oxalate is constantly more intense than the calcite one (Figure 3).

The entire reaction of the *a fresco* painted layer is a significant result from the conservation point of view, since this means that the treatment is able to completely rebuild its degraded structure.

To observe the reaction of the treatment with the plaster in the regions underneath the *a fresco* painted layer, several maps were collected in extended region of the plaster binder. In these regions, the substitution of calcite with calcium oxalate occurs at a minor extent than in the *a fresco* painted layer, as observed by the decrease of the calcium oxalate signal in FTIR maps (Figure 4) and confirmed by the averaged spectra (Figure 3) of the plaster binder collected at two different depths (100 μm and 200 μm). In general, moving towards the inner portions of the samples the intensity of the calcium oxalate bands decreases while calcite pattern becomes progressively more intense. Therefore, it is possible to assess that calcium oxalate gradually evolves from a homogeneous nucleation on the top to a less presence in the upper part of the plaster binder, and finally to spotty crystallization in the most inner part of the plaster.

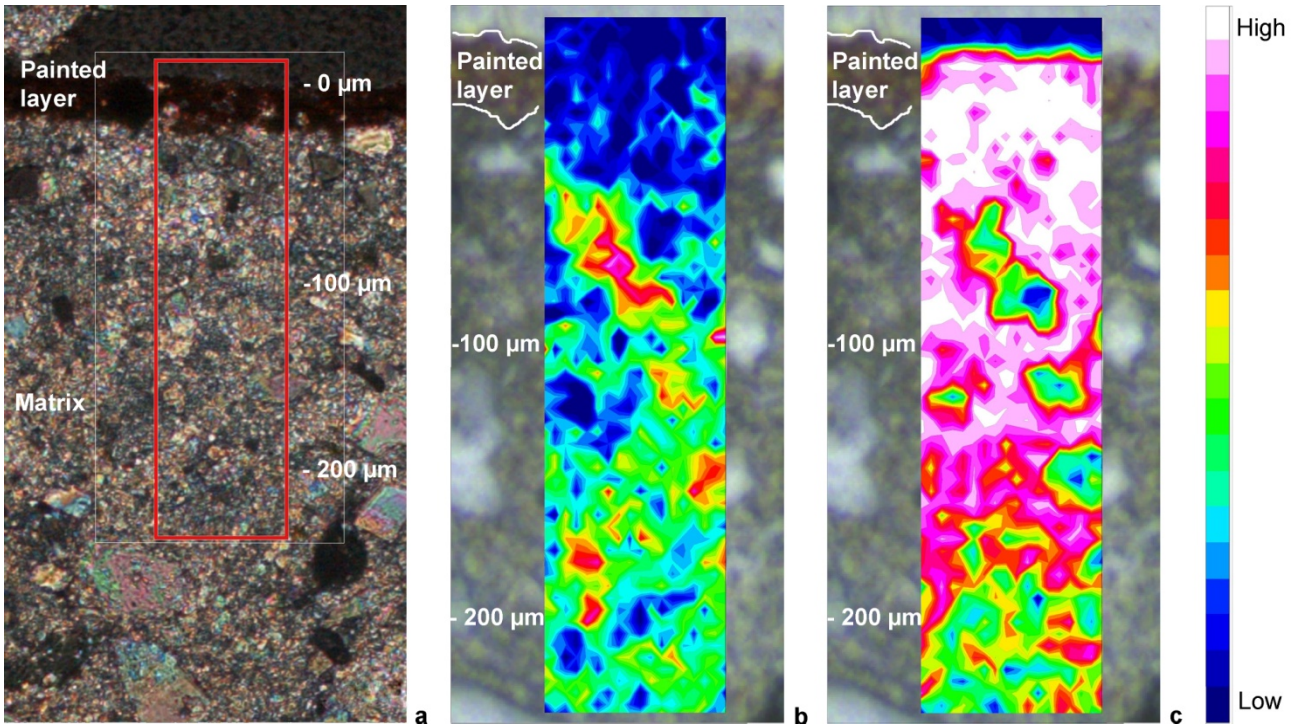

Figure 2: sample C – (a) polarizing microscope image of the mapped area (indicated with the red rectangle) and distribution maps of calcite (b) and calcium oxalate (c). The 0 µm reference depth corresponds to the top of the *a fresco* painted layer.

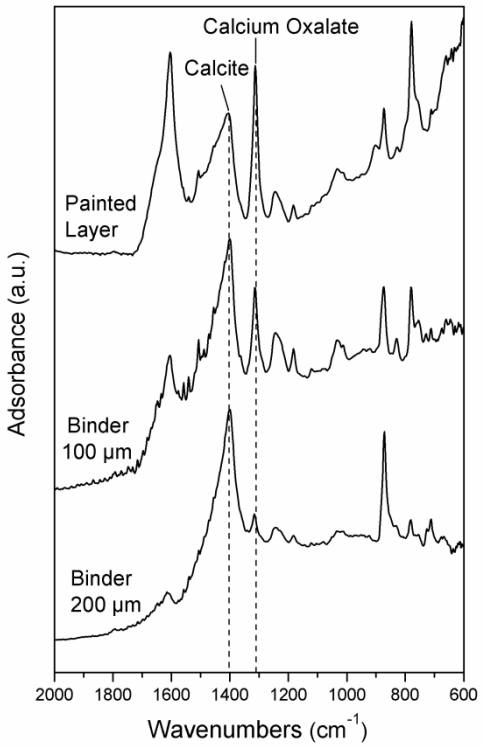

Figure 3: sample A - averaged FTIR spectra acquired in the *a fresco* painted layer and at two depths (100 µm and 200 µm) from the surface.

The depth to which calcium oxalate is formed varies with the samples, i.e. with the different treatment conditions. In particular, the homogeneous and prevalent formation of calcium oxalate in the plaster binder is up to 100 µm for sample A, 200 µm for sample B and 250 µm for sample C. As mentioned above, after these depths the formation of calcium oxalate is unevenly in isolated spots (Figure 4). Below 200 µm (sample A), 300 µm (samples B) and 350 µm (sample C) no traces of calcium oxalate were found. Where transversal fractures are present in the plaster, they act as preferential path for the diffusion of ammonium oxalate solution, which is able to reach higher penetration depth (between 500 µm and 600 µm). A further relevant aspect of the treatment diffusion has been highlighted acquiring a map at 500 µm in depth (Figure 5). In fact, it clearly shows the presence of calcium oxalate in the boundaries of the fracture as well as its nucleation from the fracture boundaries toward the lateral portion of the plaster.

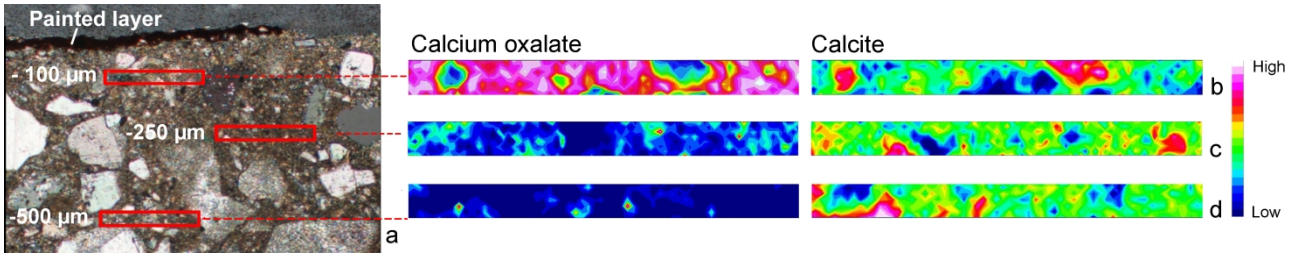

Figure 4: sample B - (a) polarizing microscope image of the mapped areas (indicated with the red rectangles) and relative distribution maps of calcium oxalate and calcite acquired at different depths from the surface: 100 µm (b), 250 µm (c) and 500 µm (d).

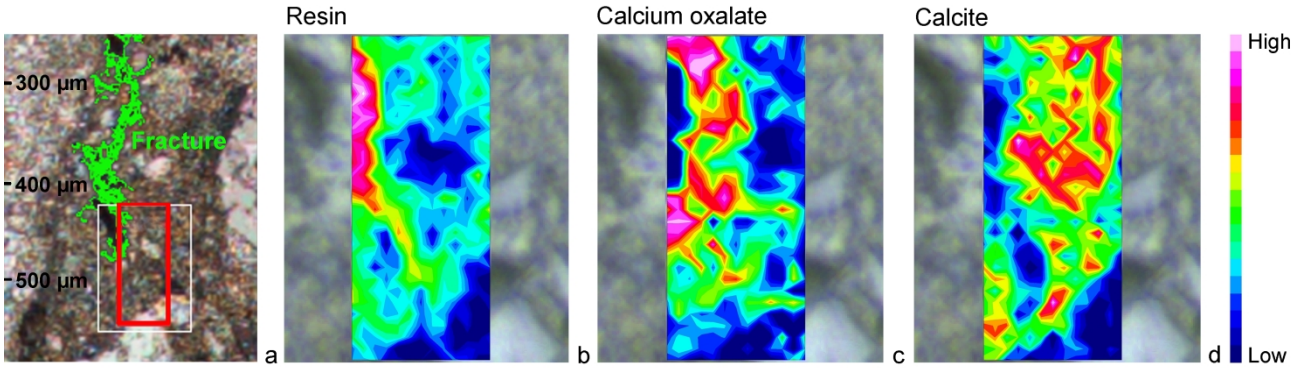

Figure 5: sample C - (a) polarizing microscope image of the mapped area (indicated with the red rectangle) with the fracture highlighted with green colour. Distribution maps of resin inside (b) calcium oxalate (c) and calcite (d).

The high lateral resolution achieved by ATR µ-FTIR allows evaluating the reaction between ammonium oxalate and the aggregate particles at the microscale; the aim is to ascertain at what extent carbonatic aggregate particles are involved with the treatment. This could be considered a

critical issue from the conservation point of view since the treatment should reconstruct just the decayed binder, and consequently a consumption of ammonium oxalate with aggregate particles is not advisable. On the other hand this reaction could ensure a stronger link between the external profile of the aggregate and the adjacent binder, making the binder-aggregate system more compact and effective.

The aggregate located in the first 100 µm (sample A) and 200 µm (samples B and C) from the external surface has completely or partially reacted with ammonium oxalate; below those depths no reaction occurs, accordingly with the broader and homogeneous plaster binder reaction. The extent of the portions involved in the reaction of the aggregate depends on its size and mineralogical composition: up to 20 µm diameter both calcite and dolomite crystals fully react; above 20 µm diameter, just some particles react in the edges (about 4-8 µm) (Figure 6). Calcite particles are more reactive than dolomite ones since the reaction takes place in a larger number of particles and at longer depth within the sample. This could be related to the different response of carbonates to the acid dissolution which takes place during the ammonium oxalate reaction: dolomite is less reactive (the conversion rate of dolomite is about eight times slower than calcite one [25]) thus the kinetics of ammonium oxalate reaction with dolomite is definitely slower compared to the calcite one.

The reaction depends also on the particles shape and on the presence of micro-fractures inside the particles: angular shape favours the reaction due to the higher specific surface area (Figure 7) and micro-fractures allow diffusing the product deeply inside the particles (Figure 8).

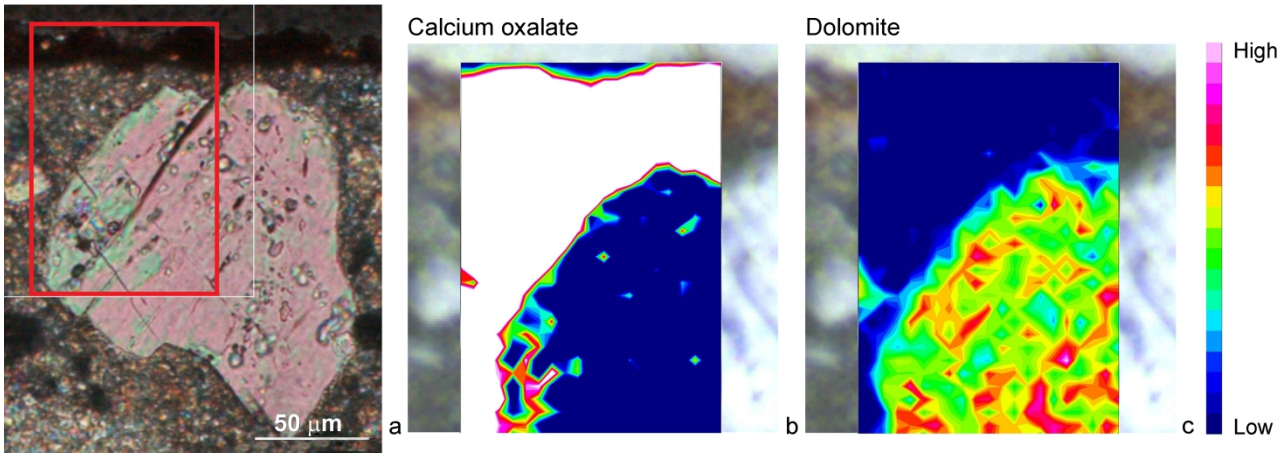

Figure 6: sample C - (a) polarizing microscope image of the mapped area (indicated with the red rectangle) and distribution maps of calcium oxalate (b) and dolomite (c). The colour scale has been set up to enhance the contrast at the edge of the aggregate particle.

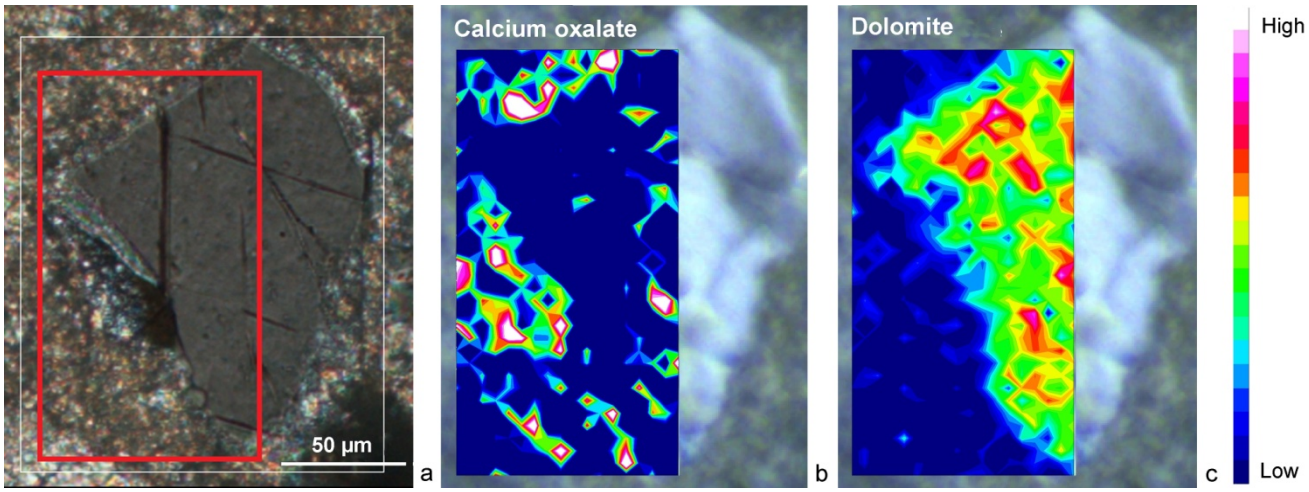

Figure 7: sample B - (a) polarizing microscope image (350 µm depth) of the mapped area (indicated with the red rectangle) and distribution maps of calcium oxalate (b) and dolomite (c).

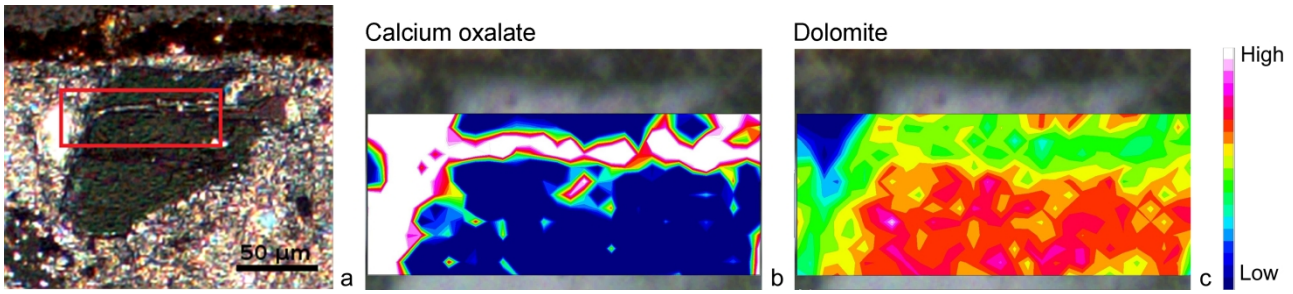

Figure 8: sample C - (a) polarizing microscope image (below the *a fresco* painted layer) of the mapped area (indicated with the red rectangle) and distribution maps of calcium oxalate (b) and dolomite (c).

Conclusions

We have presented and demonstrated the potentiality of high resolution ATR µ-FTIR mapping for the evaluation of the diffusion of ammonium oxalate treatment within painted plasters.

The observed penetration depths allow stating that the ammonium oxalate addition does not provide particular advantage. In fact, in sample A the values are even lower than sample B, treated with the same contact time and without addition. Most likely the addition favours a massive formation of newly formed phases within the first portion of the plaster and this could prevent the diffusion of treatment in the deeper parts. Sample C, treated with a longer contact time, shows the highest penetration depth; although the increment is not extremely relevant, it demonstrates that longer contact time favours the diffusion of ammonium oxalate and consequently its reaction with the inner portions of the matrix.

Even though a sporadic presence of calcium oxalates was detected below 100 µm for sample A, 200 µm for samples B and 250 µm for sample C, the actual conservation effect is limited to the areas

with an homogeneous distribution of calcium oxalates. These values allow concluding that ammonium oxalate provided a "protective" action towards the plasters.

In addition, the reaction of ammonium oxalate solutions with aggregates has been investigated and the role of fractures as preferential diffusion paths has been critically discussed.

The method extends the applicability range of conventional ATR μ-FTIR enabling to unambiguously investigate the interaction between the product and the matrix and/or aggregate particles at the microscale. The method has a wide range of potential applications in Cultural Heritage field, including the investigation of other inorganic mineral as well as organic polymer conservation treatments.

References

[1] E. Hansen, E. Dohene, J. Fidler, J. Larson, B. Martin, M. Matteini, C. Rodrìguez-Navarro, E.S. Pardo, C. Price, A. de Tagle, J.M. Teutonico, N. Weiss, Rev. Conserv. 4 (2003) 13-25.

[2] F. Casadio, L. Toniolo, J. Am. Inst. Conserv. 43 (2004) 3-21.

[3] L. Cadot-Leroux, V. Vergès-Belmin, D. Costa, J. Delgado Rodrigues, P. Tiano, R. Snethlage, B. Singer, S. Massey, E. DeWitte, Proceedings of the 9th International Congress on Deterioration and Conservation of Stone Elsevier, Amsterdam (2000), 361-369.

[4] G. Graziani, E. Sassoni, G. W. Scherer, E. Franzoni, Constr Build Mater 148 (2017) 571–578.

[5] C. Conti, C Colombo, G. Festa, J. Hovind, E. Perelli Cippo, E. Possenti, M. Realini, J. Cult. Herit. 19 (2016) 463–466.

[6] M. Realini, C. Colombo, C. Conti, F. Grazzi, E. Perelli Cippo, J. Hovind, Anal Bioanal Chem 409 (2017), 6133-6139.

[7] S. Prati, E. Joseph, G. Sciutto, R. Mazzeo, Acc. Chem. Res. 43 (2010) 792–801.

[8] F. Casadio, C. Daher, L. Bellot-Gurlet, Top. Curr. Chem. (Z) 374 (2016) 62.

[9] D. Bersani, C. Conti, P. Matousek, F. Pozzi, P. Vandenabeele, Anal. Methods 8 (2016) 8395-8409.

[10] F. Gabrieli, F. Rosi, A. Vichi, L. Cortechini, L. Pensabene Buemi, S.G. Kazarian, C. Miliani, Anal. Chem. 89 (2017) 1283-1289.

[11] S. Prati, G. Sciutto, I. Bonacini, R. Mazzeo, Top. Curr. Chem. 374 (2016) 26.

[12] I. Osticioli, G. Botticelli, P. Matteini, S. Siano, R. Pini, M. Matteini, J. Raman Spectrosc. 48 (2017) 966–971.

[13] C. Conti, C. Colombo, D. Dellasega, M. Matteini, M. Realini, G. Zerbi, J. Cult. Herit. 12 (2011) 372–379.

[14] C. Conti, C. Colombo, M. Matteini, M. Realini, G. Zerbi, J. Raman Spectrosc. 41 (2010) 1254–1260.

[15] B. Doherty, M. Pamplona, R. Selvaggi, C. Miliani, M. Matteini, A. Sgamellotti, B. Brunetti Appl. Surf. Sci. 253 (2007) 4477-4484.

[16] B. Doherty, M. Pamplona, C. Miliani, M. Matteini, A. Sgamellotti, B. Brunetti, J. Cult. Herit. 8 (2007) 186-192.

[17] D. Mudronja, F. Vanmeert, K. Hellemans, S. Fazinic, K. Janssens, D. Tibljas, M. Rogosic, S. Jakovljev, Appl. Phys. A 111 (2013) 109–119.

[18] M. Bertasa, E. Possenti, A. Botteon, C. Conti, A. Sansonetti, R. Fontana, J. Striova, D. Sali, Analyst 142 (2017) 4801–4811.

[19] D. G. Henry, J. S. Watson, C. M. John, Sediment. Geol. 347 (2017) 36–52.

[20] C. Conti, M. Casati, C. Colombo, E. Possenti, M. Realini, G.D. Gatta, M. Merlini, L. Brambilla, G. Zerbi, Spectrochim. Acta Part A 150 (2015) 721–730.

[21] D. Bikiaris, Daniilia Sister, S. Sotiropoulou, O. Katsimbiri, E. Pavlidou, A.P. Moutsatsou, Y. Chryssoulakis, Spectrochim. Acta. A. 56 (2000) 3–18.

[22] M. C. D'Antonio, N. Mancilla, A. Wladimirsky, D. Palacios, A. C. Gonzalez-Baro, E. J. Baran, Vib. Spectrosc. 53 (2010) 218–221.

[23] O. S. Pokrovsky, J. Schott, Am J Sci 301 (2001) 597–626.

[24] M. T. Domenech-Carbo, A. Domenech-Carbo, J. V. Gimeno-Adelantado, F. Bosch-Reig, Appl. Spectrosc. 55 (2001) 1590–1602.

[25] S. Schultheiss, I. Sethmann, M. Schlosser, H.J. Kleebe, Mineral Mag 77 (2013) 2725-2737.